Drone-based sensing and exploration of overhead electric power lines

Steve Mann, Samir Khaki, Jaden Bhimani, Gaël Vergès and Faraz Sadrzadeh-Afsharazar
MannLab Canada, Toronto, Ontario, Canada
mann@waterhci.com

***Abstract*—We propose a drone-based SWIM (Sequential Wave Imprinting Machine) approach to the sensing of overhead electric power lines. This will be useful in smart city sensing, e.g. to sense electric field distributions around overhead power lines without the need to stop traffic on the road as is often done with a bucket truck or lift truck that hoists utility workers up to the wires. Moreover, our remote sensing approach provides additional safety.**

***Index Terms*—Drones, sensing, electric fields, SWIM (Sequential Wave Imprinting Machine).**

Fig. 1. Testing, measurement, or maintenance of overhead power lines is usually done by a large bucket truck or stage truck to carry workers up to the power line. This operation delays traffic, blocking the road, and putting workers at unnecessary risk.

I. Background and Related Work

Measurements and maintenance of overhead power lines are expensive and disruptive. For example, when power lines are to be scanned, tested, or serviced, a large bucket truck or stage truck typically carries workers up to the overhead power line (Fig 1).

This operation typically blocks traffic on the street and also places the workers at unnecessary risk.

A. SWIM (Sequential Wave Imprinting Machine)

The SWIM (Sequential Wave Imprinting Machine) was invented in 1974 for seeing otherwise invisible phenomena such as electromagnetic waves[1], [2], e.g. radio-waves or electromagnetic radiation (EMR) in general, from AC (Alternating Current) sources. SWIM makes physical phenomena visible to the naked eye, as well as to photographic cameras. See Fig. 2 where a linear array of electric light bulbs is used as a giant paintbrush or "pushbroom" to "sweep" or "paint" the electric wave, as the array is swept back-and-forth. In a dark room with the eyes adjusted to the dark, the wave is directly visible to human observers and can also be photographed as

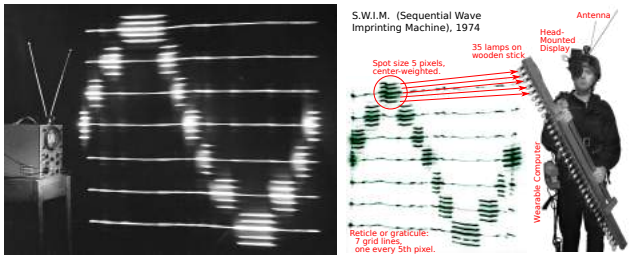

Fig. 2. Historical SWIM (Sequential Wave Imprinting Machine) photograph from 1974 of an electromagnetic radio wave from a television transmitter. The wave is made visible by an array of 35 electric light bulbs waved back and forth by hand. The bulbs are connected to a wearable computer system that includes a lock-in amplifier picking up the television signal from the "rabbit ears" antenna on the helmet. The antenna moves together with the light source, sampling and displaying the radio signal for direct viewing by the naked eye, or for photographic recording by a camera. Figure reproduced from [4].

shown in the photograph on the left half of the figure. The right half of the figure shows the experimental apparatus.

In this way, electromagnetic waves can be captured through photographs rather than merely drawn by hand or by computer graphics.

The veracity of photographs appeals to juries, judges, and courtrooms, establishing them as superior to hand-drawn sketches or computer graphics. Thus SWIM can be useful as a documentary tool, as well as for teaching, for scientific research, and as a form of visual photographic art that can be understood by a human observer, sometimes more easily or enjoyably than sketches, drawings, or computer renderings. Of course, modern SWIMs also record all the gathered data so that, in addition to the photographs, 3D computer renderings can be made in VR (Virtual Reality). Additionally, the 3D data and photographs can be combined using computational photography for 3D VR and AR (Augmented Reality) photographic overlays[3].

B. Robotic SWIM

The SWIM of Fig. 2 was often hand-held, but it was found that the result was improved by sliding the linear array of lights along a rail, and therefore the next step in the evolution of SWIM was to motorize the movement.

Thus SWIM is often embodied as a robotic mechanism for the precise scientific simultaneous sensing and display of physical phenomena[2].

978-1-6654-1394-7/21/$31.00 ©2021 IEEE

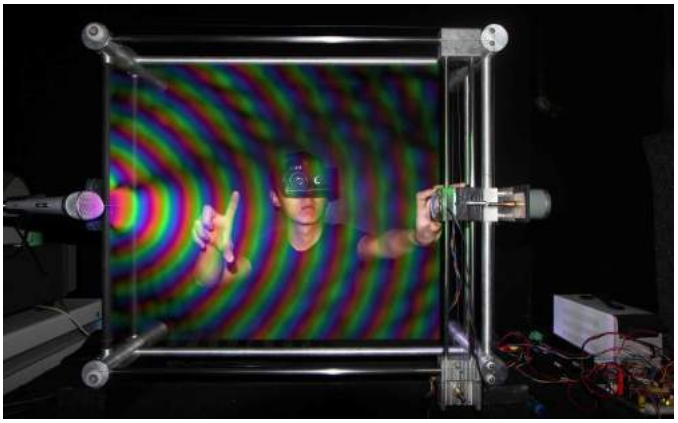

Fig. 3. Photograph of a microphone's ability to sense a 7.040 kHz sound wave. A robotic mechanism rapidly moves a loudspeaker through the space around the microphone. Attached to the loudspeaker is an RGB (Red, Green Blue) LED (Light Emitting Diode) light source. The loudspeaker is visible at the right because the camera flash that took this picture fired at the instant it was rightmost, although all the while the loudspeaker is rapidly moving around with the RGB LED. This microphone has some defects that have been made visible in the photograph. The microphone lacks sensitivity in a particular direction due to damage, and it also has a distorted phase response in that direction, facing upwards to the right, as is visible in the photograph. In addition to capturing the photograph, all of the data sensed is also captured into a 3D database for immediate viewing in VR (Virtual Reality) by way of the VR headset worn by the participant as shown in the photograph. Thus while the photograph is only 2D (2 dimensional) the participant can see and interact in 3D (3 dimensions). Figure reproduced from [2].

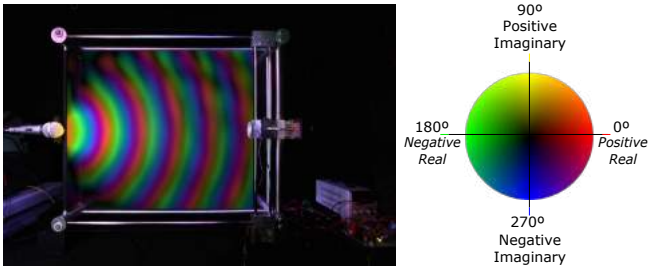

Fig. 4. Photograph of the microphone sensing at a different frequency, this time lower (3.52 kHz). Note the longer wavelength of sound and compare it with that of Fig 3. The RGB LED that moves with the loudspeaker is driven by the output of the lock-in amplifier feeding a converter from (real, imaginary) coordinates to RGB (Red Green Blue) as illustrated. Figure reproduced from [2] and colour wheel adopted from [4].

As an example of how SWIM has been used in the past (previously reported in the literature[2]), consider a microphone which is a device that can sense sound waves.

The capacity of a microphone to sense these sound waves is something that can be made visible to the naked eye or photographic cameras. This visibility takes the form of a veillance wave function [5], which is a complex-valued function of space. See Fig. 3 and 4.

Sound waves travel at the speed of sound but the lock-in amplifier of the SWIM produces waves that sit still:

> Whereas the standing wave stands still only at the nodal points... the sitting wave remains approximately fixed throughout its entire spatial dimension, due to a sheared spacetime continuum with time-axis at slope 1/c. The effect is as if we're moving along at the speed, c, of the wave propagation, causing the wave to, in effect, "sit" still in our moving reference frame[5].

Sitting waves are complex-valued functions often represented using colour to denote phase[1], [2].

To represent phase, an algorithm from [2] was adapted to implement the colours shown in [4]. The algorithm works by dividing the Argand plane (the complex plane) into three regions: [0 to 180°), [180°to 270°), and [270°to 360°). A cross-fade is then calculated according to which region the angle is in red-green, green-blue, or blue-red for each region respectively. The values thus obtained are then multiplied by the lock-in amplifier's output normalized to the [0,1] interval. These values are in turn multiplied by 255.99, and the result converted to unsigned character byte values [0 to 255], thereby yielding R, G, and B values respectively. A visual depiction of this is shown in Fig. 4 where the resulting colour wheel is superimposed upon the Argand plane.

Being able to see and photograph sound waves is useful. For example, we discovered (saw) and photographed a defect in a microphone (Fig. 3). Note the dark region from the microphone toward the upper right at about a 30-degree angle (the direction a clock hand would take facing 2 o'clock).

Visualizing sound waves is often done in virtual environments [6], [7], [8] and is well known in art. But with SWIM we now have photographic evidence of the defect. SWIM produces both photographic evidence as well as data that can be explored using a VR headset for example, rather than just the data alone.

To understand how SWIM can be used to see and photograph wave phenomena, see Fig. 5 which is a photograph of two functioning (no defects) Shure SM58 microphones.

C. Drone-based SWIM

This paper builds upon research reported in[9] which introduced the idea of using drones for sensing and metasensing (the sensing of sensors and the sensing of their capacity to sense). Previous work on using drones for sensing and metasensing was primarily focused on optical sensing and optical metasensing (e.g. the sensing of optical sensors), such as photographing and characterizing or measuring, a camera's capacity to sense.

II. Overview

In our case, we use a drone to move a sensor or measurement device together with an RGB LED that displays the measured quantity, as shown in Fig. 7. Our measurement device is an electromagnetic probe that functions as an antenna. Our experimental setup consists of a miniature model of a city built at approximately 1/30th scale, having overhead power lines that are connected to a 3-phase signal generator as shown in Fig. 6.

We conducted tests at various frequencies and found that at all the frequencies we tested, even a very faint signal can be received with the lock-in amplifier. The SYSUxMannLab

Fig. 5. Photograph of the interference patterns between the capacity to sense of a matched pair of Shure SM58 microphones. The SWIM apparatus (e.g. lock-in amplifier, etc.) is also visible in the picture. Figure reproduced from[2].

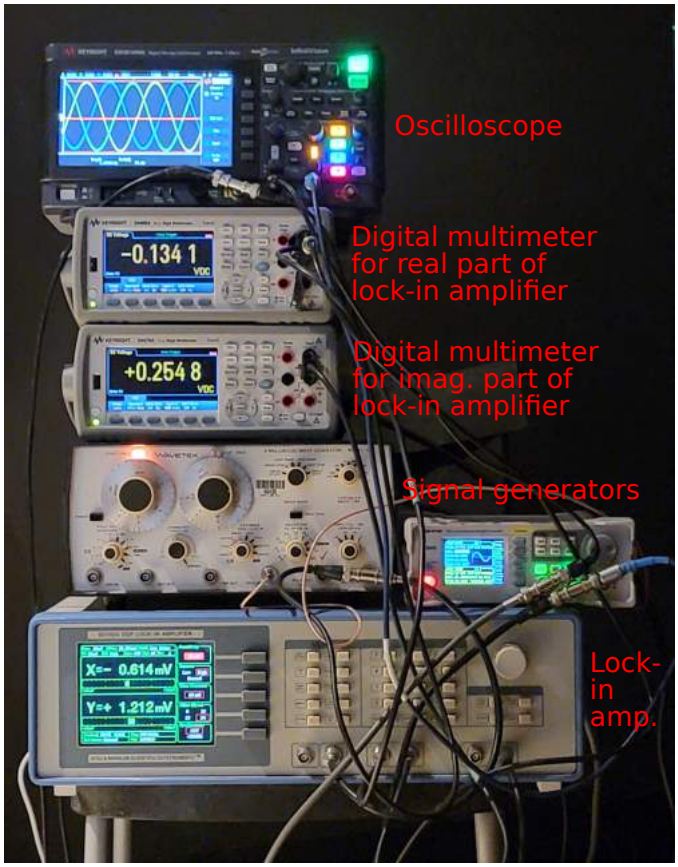

Fig. 6. Test equipment stack of the experimental setup. A Wavetek MODEL 185 signal generator produces a sinusoidal waveform for one of the 3 phases, and a Wavetek MODEL 205 signal generator provides the other two phases in sync. with the first. A SYSUxMannLab Model 1024SO Scientific Outstrument™ (multicomponent lock-in amplifier) has its reference input driven by the first phase of the WAVETEK 185. The signal input of the lock-in amplifier is fed from the antenna probe on the drone. The real and imaginary analog outputs of the lock-in amplifier are fed into two Keysight 34470A digital multimeters which convert the analog signals to digital, which are then passed over a serial port to the laptop computer acting as our ground control station.

Model 1024SO that we are using offers a gain of up to 10^9 and a dynamic reserve of 120dB (i.e. noise voltage can be 10^6 times stronger than the signal).

In our experiments, we initially used a frequency of 60Hz which has a wavelength of 5,000km for testing but then adjusted the frequency upwards to match the reduced physical scale. As our model is about 1/30th scale, we also tried frequencies like 1800Hz, 2kHz, etc. We found that the results did not depend strongly on frequency in the sense that the wavelength was always significantly larger than the physical space we were exploring. A frequency of 1kHz was used at last to generate the three phases. The sensitivity range of the lock-in amplifier was set to 2mV and its time constant was set to 30ms. The real and complex outputs of the lock-in amplifier were digitized using an analog-to-digital converter. The magnitude and phase of the sensed signal were computed and converted to an RGB value according to the algorithm depicted in Fig. 4, rightmost. The RGB data were then transmitted to be displayed on an RGB LED on the drone. The drone-based power line sensing schematic is depicted in Fig. 7.

Unlike other robotic movement devices for SWIM, drones offer a critical advantage as they operate autonomously, require minimal external hardware setup for positioning, and they can fly into confined or hard-to-reach spaces that robots sometimes have difficulty reaching. Once the drone's position has been calibrated, it can trace out electromagnetic waves or other quantities with centimetre level precision.

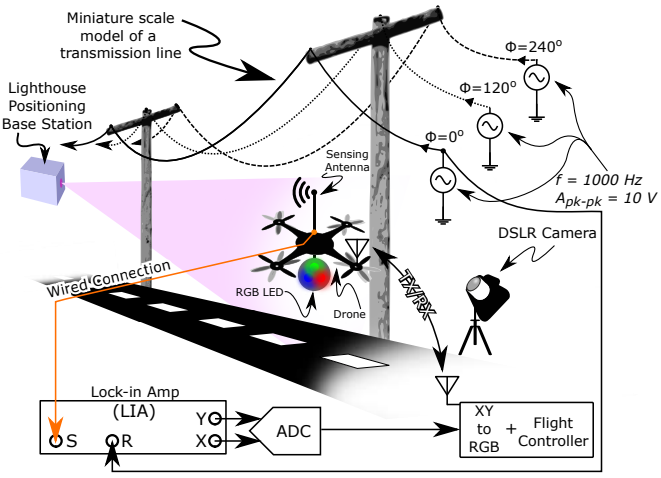

Fig. 7. Schematic representation of the drone-based power-line sensing.

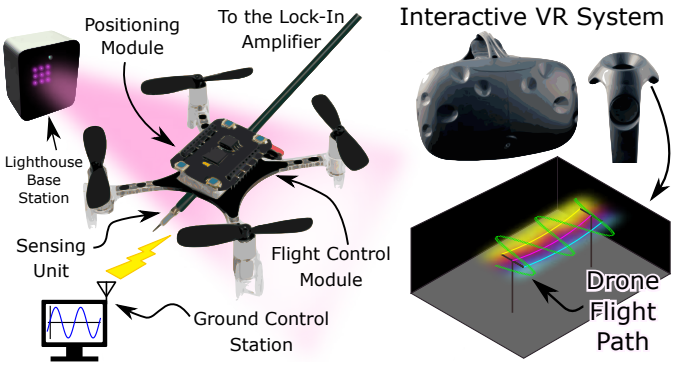

Fig. 8. Overall drone system for sensing overhead electrical power lines. The main components from Section III-A are identified, as well as the Interactive VR System for an immersive reality experience of the drone's sensing.

III. Exploring Drone-based sensing

The components of our drone system are outlined in the schematic in Fig. 7.

A. Components

Our drone system consists of the *Positioning Module* (lighthouse base station and the lighthouse deck attached to the drone), *Ground Control Station* (laptop), *Sensing Unit* (antenna) and the *Flight Controller* (main circuit board of the drone), all of which have been applied to the Bitcraze Crazyflie 2.1 drone[10]. This system forms a closed feedback loop enabling the drone to traverse the 3D space with centimetre-level precision.

1) Positioning Module: The Crazyflie drone uses Cartesian positioning in which users can specify a target setpoint in space for the drone to navigate towards rather than a direction or heading[11]. To create the Cartesian space in which the drone can fly, we connected a Vive lighthouse base station [12] that communicates with the drone's lighthouse positioning deck through IR (Infrared) light. The base station covers a range of 12 metres with a conical radius of 120 degrees[11]. The deck, fastened on the drone, contains four TS4231 receivers positioned on the corners enabling positional control over space[13]. Within each TS4231, the IR signal is detected via an IR photo-diode and amplified using a differential transimpedance amplifier. After noise is filtered out, the signal is converted from analog to digital and output via two pins labelled D and E on the drone. The base station sweeps the environment with the IR light, triggering the sensors on the deck. The delay and intensity of each sensor's signal reception allow the drone to estimate its relative angle and distance to the base station[14]. The output data enables the rendering of a 3D Cartesian coordinate system with the origin at the drone's initial position. The rendering indicates the drone's current position relative to the environment, at a scale of 1:1 between each virtual unit and real metre. The advantage of the generated Cartesian Space is a high level of precision in positioning which allows for better interpolation of measurements taken along a flight path than could have been obtained using a heading-based system.

2) Ground Control Station: To determine the flight path of the drone, a ground control station was established using a laptop that connects via RF (radio frequency) with the drone. The laptop generates a sinusoidal raster over the region of interest in python. A software-defined iterative loop is created to increment the drone's position along the raster creating a highly defined flight path of the form $x(t) = A\sin(f * t)$ with over 18000 recorded data points over the region of interest. The positioning instructions were passed to the drone through the crazyflie-clients-python (cflib) via the crazyradio PA (public address) USB dongle. The X and Y Positional instructions were encoded based on the above defined waveform[15]. The Z position of the drone was predetermined as a constant 95 centimetres in order to fly exactly 5cm above the power lines, close enough to detect the generated electric field generated while far enough to avoid crashing into the power lines.

3) Sensing Unit: For remote sensing, the drone contains a sense-response system made of the antenna and LED ring forming the sensing module[16]. The input measurements from the antenna create an output response on a ring of 12 RGB LEDs[16] as the drone traverses through space and time. The antenna is fastened to the bottom of the drone allowing it to fly over the wires and collect measurement data. The measured data is displayed on the LED ring for capture by way of time-exposure photography, as is typical with SWIM. The SWIM device made from the coaxial cable and LED ring transforms the measurement data into the visible spectrum. SWIM devices often use colour to represent different states of a wave (e.g. phase).

The antenna measures the real and imaginary components of the field and passes them through the lock-in amplifier and to the two Keysight multi-meters, the phase angle between the two is calculated as $\arctan(\text{imaginary}/\text{real})$ and the magnitude as $\sqrt{\text{real}^2 + \text{imaginary}^2}$. A specific colour is then obtained as dictated by the colour wheel shown in Fig. 4. With regards to RGB intensity, the magnitude is transformed to magnitude$^{3.5}$ to compensate for line-to-line interference when the magnitude is lower. The exponentiation allows a fall-off of colour intensity when the magnitude in a specific line is recorded to be low – irrespective of interference from nearby wires, thus forming a compametrically true and accurate noise-gate effect[17]. The product of the adjusted magnitude and phase correspondence allows one to set the RGB value of the LEDs.

4) Flight Controller: The drone's flight controller consists of an STM32F405 microcontroller [10] which parses the data from the lighthouse deck, onboard gyroscope and onboard radio receiver to send specific voltages to each of the four motors and maintain a consistent position in 3D space. Once a setpoint is sent by the python client, the flight controller changes the voltage supply to each specific motor enabling it to navigate through space [10]. As it traverses the space, it uses a constant feedback loop with the lighthouse deck and the base station to determine its current position and update the voltage supply to each motor until it reaches the setpoint.

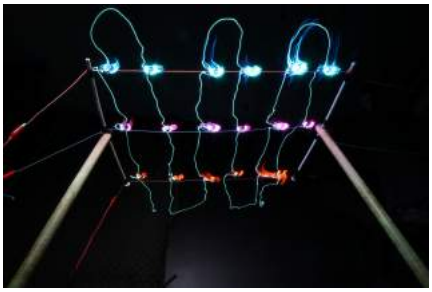

Fig. 9. Photograph of drone flying a raster pattern with changing LED colours to depict the sensed electric field. One individual LED was coloured green at all times to illustrate the drone's flight path. All power lines are fed by continuous-wave alternating current such that the electric fields of all three wires remain constant in relation to the reference signal of the lock-in amplifier over the drone's flight path.

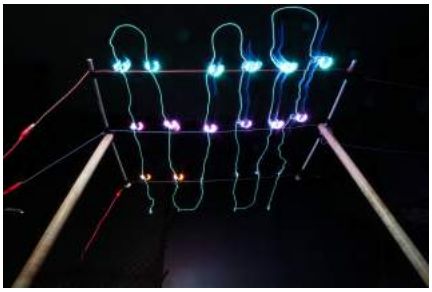

Fig. 10. Similar to Fig. 9. The wire furthest from the camera was cut. Thus, the absolute value of the real and imaginary components of the electric field detected past the wire's cut approximated zero, causing the RGB value of the drone's LEDs to result in black.

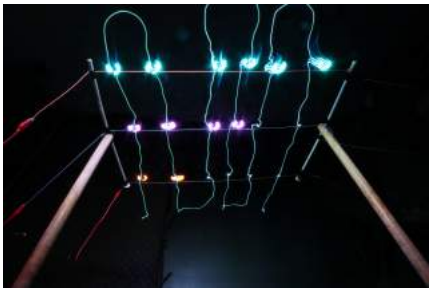

Fig. 11. Two wires were cut. This caused the absolute of the real and imaginary components of the electric field to be zero and the drone LEDs to be black on the wires post-cut.

B. Capabilities of Sensing

In applying the drone systems to power line sensing, we introduced the drone's capacity to sense using *Phase Sensing* and *Defect Sensing*.

1) Phase Sensing: Phase Sensing details the capacity for the drone system to sense properly working power lines. When power lines are connected, the drone system provides verification through a sense of uniformity with both photographic evidence and the generation of a 3D VR data-set that can be explored visually and computationally.

2) Defect Sensing: The case of Defect Sensing improves upon the standard capacity presented in *Phase Sensing* by being able to detect irregularity in the sensed medium. For power lines, we consider this to be a discontinuity in the path of electrical current propagation represented as a break in the wire. The drone system, in response to this disruption, provides photographic evidence as well as data visualization (VR) representation of the difference in regions between regular and irregular sections.

IV. Testing Drones for Power Line Sensing

Our proposed methodology for power line sensing using drones has been tested using a controlled environment to further bolster the efficacy of this approach. The overall testing phase can be broken down into the following sections: Miniature Model Design Choices, Test Methodology, and Test Results.

A. Miniature Model Design Choice

The simulated test was constructed to model general power lines and test the drone's ability to sense these lines and display meaningful interpretations of the data in both a photographic and 3D VR visual representation.

1) Power Line Characteristics: In constructing the miniaturized model, we had 3 equally spaced parallel power lines. In city-scale power systems, power lines run for miles without termination as to effectively deliver power to as many people as possible with as few junctions as possible. To simulate this and get a more realistic depiction of the electric field around a line, the wires carrying the three-phase power generated by the signal generators were hung between the two power poles and were continued on for several more metres before being hung on the opposite end of the room. From a physics perspective, extending the wires beyond their endpoints was done purposefully as to prevent destructive interference between the three equidistant wires in a three-phase system.

B. Test Methodology

To test the sensing of the drone, we employed the following tests: *Manual Testing* and *Flight Testing*. The *Manual Testing* is used to demonstrate the capabilities of the drone in sensing and differentiating different mediums – it helps to visualize the full extent of what the drone can sense in the environment. The purpose of this type of testing is to build the case for drone-based sensing of the electrical power lines. The *Flight Testing* demonstrates how the drone performs using the current equipment and setup. Ideally, the best *Flight Testing* should approximate results from the *Manual Testing*.

1) Manual Testing: The manual testing procedure is used to illustrate the effectiveness of the drone's capacity to sense. By attaching the drone to a metre stick and sweeping it across the power lines in a tight raster, long exposure photography reveals what the drone sensed under controlled conditions. The colour of the on-board LEDs changed in accordance with the phase-sensitive detection of the electric field by the *Sensing Unit* - described in Section III-A3. This is used as a benchmark for what the drone should be able to detect autonomously in the *Flight Testing*. As seen in Fig.'s 9, 10, 11, the drone displayed a high luminosity when it was directly over the electrical lines, however in the spaces between, it dims to black – thus being able to accurately sense the electrical field.

2) Flight Testing: The flight testing consists of flying in a raster pattern above the power lines without human interference/interaction. Long exposure photography is used to reveal what the drone sensed. The flying drone cannot be too close to the power lines due to the risk of collisions and therefore

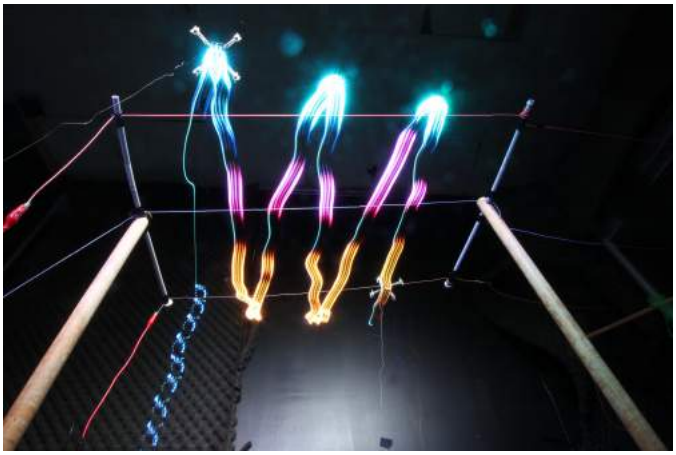

Fig. 12. Features the drone flight field test, where the drone flies over the fully connected power lines in a raster pattern, visually illuminating regions of electrical power line electric field presence.

some of the results may display a margin of error that can be minimized using an antenna array as the sensing instrument [18].

C. Test Results

The miniaturized power lines described above were used as a proof of concept test for the proposed drone-based sensing. The model provides adequate resemblance to the real environment thus giving an accurate representation of how the drone would perform in a real-environment setting. The drone's capacity to sense was explored through the *Manual Testing* in Section III-B with results in Fig.'s 9,10, and 11. In 9, the current remained continuous between the two poles. In 10, the wire furthest from the camera was cut following the first cycle of the drone's path, causing there to be a discontinuity about one third of the way down the wire. Similarly in 11, the wire furthest from the camera was cut, in addition to the centre wire being cut following two cycles of the drone's path, causing a discontinuity approximately two thirds of the way down the wire.

As seen by the progression of photos, the drone system is able to detect discontinuities along the power lines. When the drone flies over a continuous region of the power line, it illuminates colours in accordance with the detected phase. When it is in between or past the wires, it dims to black as it is able to differentiate the interference from direct detection of the power line. Once the drone passes a discontinuity in the wire, it is able to sense the lack of electrical transmission thus resulting in a dimming to black. This result demonstrates the applicability of drones in power line remote sensing. Figure 12 showcases the drone's phase-sensitive and in-flight sensing of the electric field present around the miniature three-phase transmission line.

V. Conclusion

In this paper, we introduced a novel approach to the sensing of electrical power lines. The presented method offers advantages in safety and convenience by the integration of remote sensing through drones. The veracity of photographs produced through SWIM-type output from drone sensing provides confirmation-based evidence of the electrical characteristics of the power lines along with the 3D database that can be used for VR (Virtual Reality) exploration in addition to the photographs. The demonstrated results from *manual* confirmation as well as *flight tests* further support the efficacy and versatility of the proposed drone system for wide-scale adoption in the field of electrical power line sensing, testing, and exploration.

References

[1] S. Mann, "Wavelets and chirplets: Time–frequency perspectives, with applications," in *Advances in Machine Vision, Strategies and Applications*, world scientific series in computer science - vol. 32 ed., P. Archibald, Ed. Singapore . New Jersey . London . Hong Kong: World Scientific, 1992.

[2] S. Mann, "Phenomenological Augmented Reality with SWIM," pp. 220–227, IEEE GEM2018.

[3] S. Mann, R. Janzen, T. Ai, S. N. Yasrebi, J. Kawwa, and M. A. Ali, "Toposculpting: Computational lightpainting and wearable computational photography for abakographic user interfaces," in *IEEE CCECE 2014*.

[4] S. Mann, ""Rattletale": Phase-coherent telekinetic imaging to detect tattletale signs of structural defects or potential failure," *SITIS 2017, SIVT4: Theory and Methods*.

[5] S. Mann, "Surveillance, sousveillance, and metaveillance," pp. 1408–1417, CVPR2016.

[6] S. Redfern and J. Hernandez, "Auditory display and sonification in collaborative virtual environments," *SFI Science Summit (Dublin)*, 2007.

[7] H. G. Kaper, E. Wiebel, and S. Tipei, "Data sonification and sound visualization," *Computing in science & engineering*, vol. 1, no. 4, pp. 48–58, 1999.

[8] D. R. Begault and L. J. Trejo, "3-d sound for virtual reality and multimedia," 2000.

[9] M. Steve, P. Cayden, H. Jesse, L. Qiushi, Z. Bei Cong, and X. Yi Xin, "Drone swarms for Sensing-of-Sensing," *IEEE Sensors*, pp. 1–4, Aug. 2019.

[10] "Datasheet crazyflie 2.1 - rev 1." [Online]. Available: https://www.bitcraze.io/documentation/hardware/crazyflie_2_1/crazyflie_2_1-datasheet.pdf

[11] "Lighthouse positioning system: Dataset, accuracy, and precision for uav research." [Online]. Available: https://arxiv.org/pdf/2104.11523.pdf

[12] "Lighthouse system overview." [Online]. Available: https://www.bitcraze.io/documentation/repository/crazyflie-firmware/2021.03/functional-areas/lighthouse/system_overview/

[13] "Lighthouse positioning deck." [Online]. Available: https://www.bitcraze.io/documentation/hardware/lighthouse_deck/lighthouse_deck-datasheet.pdf

[14] "Ts4231 light to digital converter." [Online]. Available: https://triadsemi.com/wp-content/uploads/2019/09/TS4231-Datasheet.pdf

[15] "The crazyflie python api." [Online]. Available: https://www.bitcraze.io/documentation/repository/crazyflie-lib-python/master/user-guides/python_api/

[16] "Led-ring deck." [Online]. Available: https://www.bitcraze.io/documentation/hardware/led_ring_deck/led_ring_deck-datasheet.pdf

[17] S. Mann, "Comparametric equations with practical applications in quantigraphic image processing," *IEEE Trans. Image Proc.*, vol. 9, no. 8, pp. 1389–1406, August 2000, iSSN 1057-7149.

[18] S. Wei, L. Zhang, W. Gao, and Z. Cao, "Non-contact voltage measurement based on electric-field effect," *Procedia engineering*, vol. 15, pp. 1973–1977, 2011.